Synthesis and Characterization of Three-Phase Polymer-Graphene Oxide-Ceramic Composites

Muhammad Saleem Khan*, Mohammad Sohail, Noor Saeed and Ayesha Afridi
National Center of Excellence in Physical Chemistry, University of Peshawar (25120), Pakistan.
saleemkhan@upesh.edu.pk*

(Received on 29th July 2015, accepted in revised form 21st December 2015)

Summary: In this study, novel three-phase hybrid (inorganic-organic) composite comprising $Fe_{0.01}La_{0.01}Al_{0.5}Zn_{0.98}O$ ceramic particles (FLAZPs), conducting polymer polyaniline (PANI) and grapheme oxide (GO) was synthesized. The ceramic particles were produced by sol-gel technique. For the homogeneous dispersion of FLAZPs particles in the PANI matrix, *in-situ* free-radical polymerization of aniline (PANI precursor) was performed. FLAZPs distributed in the matrix during the polymerization process. GO was synthesized via modified Hummer's method which was then blended with two-phase composite using simple one-pot blending technique. The prepared materials were subjected to FT-IR, TGA, XRD and SEM to analyze their physical properties. FT-IR showed the successful complexation of the materials with one another. XRD confirmed the crystalline nature and phase distribution in the composites. FLAZPs enhanced the thermal stability of PANI and GO in the composites. SEM showed that ceramic particles are in the range from micro to nanometer and are well dispersed in the PANI matrix in two-phase composite. Furthermore, GO prevented the agglomeration of particles while interacting with PANI in the three-phase composite. Extensive dielectric studies were carried out which showed that PANI and GO have about the same additional effect on various dielectric properties of FLAZPs. The *AC* conductivity ($\sigma = 7.79 \times 10^{-1}\ \Omega^{-1}cm^{-1}$) achieved by two-phase and three-phase composites is much higher in comparison to pure FLAZPs ($\sigma = 3.17 \times 10^{-1}\ \Omega^{-1}cm^{-1}$).

Key words: Hybrid composites, TGA, SEM, XRD, Dielectric properties.

Introduction

During the past two decades, inorganic/organic composite materials have gained much attention in the field of nanotechnology due to their excellent electrical, mechanical, optical, thermal and magnetic properties [1-4]. They have wide applications in LEDs [5], photochromic devices [6], solar cells [7], contact lenses [4], thin film transistors [8], corrosion protection coatings and optical wave guiders [9]. Polymer-ceramic composites are prominent candidates in this regard. Individual components of such composites often face limitations in their applications due to their low thermal, electrical and mechanical properties. One of the best solutions to this issue is to hybridize these materials with one another in the form of composites, thus modifying or reinforcing one another for suitable applications. Novel properties are exhibited by these composites when fabricated in optimized fractions [10].

The distinctive features of ceramics (e.g., low cost, relative abundance) and that of polymer matrix (e.g., light weight and ease of synthesis) impart special characteristics (e.g., stiffness, enhanced impact strength, permeability, refractive index and wide adsorption behavior) to these composites. The blending of ceramic (inorganic) particles with polymers has a strong synergistic effect. The stiffness and strength of a polymer can be increased by the introduction of inorganic fillers. Silica (SiO_2) and zinc oxide (ZnO) particles are used to improve impact strength and UV stability of the composites respectively, while magnesium carbonate ($MgCO_3$) particles have been used to develop flame retardancy in these materials [11]. The interaction of inorganic particles (fillers) with polymers results in the development of the interfacial polymer shells. The presence of such shells not only reduces the filling degree of the fillers in a polymer matrix, but also affects the physical properties of the polymer by decreasing their mobilization. As a result, electrical, magnetic thermo-mechanical as well as the optical properties of the composites is improved [12]. Owing to the synergism among the properties of the components, these hybrid materials display significant change in thermal, mechanical, magnetic and electrical properties. Three-phase Polyimide/$BaTiO_3$/Ag composites have shown enhanced dielectric properties [13]. Polymer composites reinforced with ceramic nano-fillers and carbon nanotubes have been studied widely for their electrical, photocatalytic and anti-bacterial activities [14, 15]. In these composites transition metal ions act as dopants for electrical behavior while the conducting PANI works as sensitizer and improves the light absorption properties. Graphene based polymer nanocomposites have been found to be useful for the suppression of electromagnetic

*To whom all correspondence should be addressed.

interference (EMI) in electronics and transient power sources. Recently few layer graphene/poly vinyl alcohol composite sheets have been used as EMI shielding through the absorption mechanism [16]. Composites of epoxy resin with carbon nanotubes (CNTs) as fillers have also been analyzed for their microwave absorbing properties [17]. Layered graphene has been investigated as a suitable anode material for Lithium ion batteries [18]. Graphene oxide (GO), the oxidized form of graphite, have efficient thermal and mechanical properties and is used as re-enforcing agent in these composites. Ternary composite GO/PANI/Fe_3O_4 has shown enhanced microwave absorption properties [19]. Because of GO's amphiphilicity, it has been used as Pickering stabilizing agent in the synthesis of macroporous GO-polymer composites [20]. GO based CuO composite has been used as electrode material in non-enzymatic glucose detection [21]. GO modified Li_2FeSiO_4/Carbon composite has been proposed to show enhanced electrochemical performance as cathode in Li ion batteries [22].

In this paper, our synthesized ceramic-PANI two-phase composites combine the advantages of dopants (metal ions) and light sensitivity and conductivity of PANI. PANI has added effect on the dielectric properties of ceramic particles. Effect of GO on various properties of the prepared three-phase composites has also been studied.

Experimental

Materials

All the chemicals, Ferric nitrate, zinc nitrate, graphite powder, sulfuric acid (Scharlu, Spain), lanthanum nitrate (Merck, PAK), aniline (Acros Organics, USA), citric acid (Daejung, Korea) and potassium permanganate, potassium nitrate (BDH, England) were of analytical grade and were used as received without further purification. For all the synthesis procedures, the conditions (e.g. Concentration, temperature, pH) were optimized.

Methods

Synthesis of FLAZPs

The $Fe_{0.01}La_{0.01}Al_{0.5}Zn_{0.98}O$ ceramic particles were prepared via sol-gel technique. In a typical experiment, $Fe_2(NO_3)_3{\cdot}9H_2O$ (0.073g), $La(NO_3)_3{\cdot}9H_2O$ (0.162g), $Al(NO_3){\cdot}3H_2O$ (1.242g) and $Zn(NO_3)_3{\cdot}6H_2O$ (11.552g) were dissolved together in 100 ml de-ionized water (pH = 7, σ = 0.51 μScm^{-1}) under magnetic stirring (500 RPM). Citric acid (5g) was added slowly to this mixture. Liquid ammonia was added drop wise to keep the pH of the solution neutral. After one hour continuous stirring, the solution was then kept in an oven for drying at about 80°C. A light bluish gel was obtained which was then ground and sintered for 3 hours at 600°C. After cooling to room temperature, the obtained diffused material was ground properly in an agate mortar for half an hour to get particles in micro to nano dimensions. These were assigned with the sample ID A1.

Synthesis of A1-PANI two-phase composites

For the incorporation of A1 particles in polymer (PANI) matrix, *in-situ* free radical polymerization route was adopted. In 100 ml de-ionized water, 250mg A1 particles were dispersed under stirring. Subsequently, 25 ml of aniline solution (10% in 1 M HCl) and 25 ml of ammonium persulphate (0.1 M in I M HCl) were added to this suspension drop wise. The reaction mixture was then stirred for 3hours in an ice bath (0-5°C) following overnight digestion. For removing soluble impurities and side products, the sample was centrifuged (4000 RPM) for 10 minutes twice and was dried in an oven at 70°C. The obtained composite was assigned with sample ID A2.

Graphene Oxide (GO) Synthesis

GO was synthesized via modified Hummer's technique [23]. In a set of experiment, a glass beaker was placed in an ice bath. A 25 ml H_2SO_4 (98% w/w) was taken in the beaker and 0.5 g graphite flakes were added slowly to it Then about 0.5 g KNO_3 were mixed to this suspension and it was kept under magnetic stirring. After about 20 minutes, $KMnO_4$ (3g) was slowly added to the mixture. Then the beaker was transferred to a 35 ^{0}C water bath and the solution was stirred for 1hour. A thick dark paste was produced. Then 100 ml de-ionized water was added to this paste and stirred at 90 ^{0}C for half an hour along with slow addition of 30% H_2O_2. The warm solution (Dark brown to yellow) was then filtered and washed with 100 ml de-ionized water. The filtered cake was then dispersed in water through mild sonication for 1hour. Suspension obtained was then centrifuged (4000 RPM) for 10 minutes twice. The supernatant that contained small GO pieces and water soluble byproducts was discarded. Ultimately, the solid GO powder was obtained from the sediment under air-dry.

Synthesis of A1-PANI-GO three-phase composites

For the synthesis of A1-PANI-GO composites, 200mg of A1/PANI and 100mg of GO were dissolved separately in 60 ml and 40 ml de-ionized water respectively. Both the solutions were

stirred for 30 minutes. Then GO solution was added to the composite solution and the mixture was re-stirred for 4 hours. Then it was kept for drying at 70°C for 24 hours. This resulted in the formation of three-phase composite A3. The typical composition of these composites during synthesis is given in Table- 1. The flow sheet represents the whole synthesis procedure.

Table-1: Concentration of constituents in the prepared composites.

Sample	FLAZPs concentration	PANI concentration	GO concentration
		(mg ml^{-1})	
A1	10	1	Nil
A2	3.3	3.3	2.5

Characterization

FT-IR spectroscopy studies were carried out using (IR Prestige-21). Scanning electron microscope (SEM) (JEOL JSM- 6700F) was used for surface morphologies and particle dimension detection using samples stabs on electro-active disks. Thermal studies were conducted using TG/DTA Diamond (Perkin Elmer, USA) in a nitrogen environment at 10 ^{o}C heating rate. Phase distribution and crystallinity of the composites were studied by XRD (JDX-3532 JEOL Japan) technique. Dielectric properties were analyzed using RF Impedance/Material Analyzer (Agilent E4 997 A) in the frequency range from 1MHz to 3GHz at ambient temperature.

Results and Discussion

Fourier Transform Infrared Spectroscopic (FT-IR) study

FT-IR analysis shows the formation of ceramic micro-particles and their compositing with PANI and GO in Fig. 1 while Table-2 represents the peak positions of different bands of specific intensity with their assignments. Broad peaks at 3370, 3506 and 3516 cm^{-1} represent O-H stretching modes in A1, A2 and A3 respectively. The starting peak at 410-430 cm^{-1} denotes Zn-O stretching mode in A1 ceramic particles. The characteristic peaks of A2 obtained in the spectrum are 621 cm^{-1} for C-C bonding in aromatic ring, 1070 cm^{-1} for C-H out of plane bending in benzenoid ring, 1284 cm^{-1} and 1480 cm^{-1} for C-N stretching modes in benzenoid and the neighboring quininoid rings respectively and 3005 cm^{-1} represents symmetric stretching vibration of methyl and methylene groups in the two-phase composite [14]. In the three-phase composite A3, the strong peak at 3516 cm^{-1} is due to O-H stretching vibration of C-OH at the GO surface, 1710 cm^{-1} is due to C=O stretching vibration of COOH in GO while peak at 1060 cm^{-1} is attributed to metal-oxygen bond stretching in the composite [24]. The absence of any apparent peak in A2 and A3 in the region from 2900 to 1720 cm^{-1} as compared to A1 shows that the particles are successfully dispersed in PANI/GO matrix. This shows that the free functionalities have been occupied by the entering entities in the composites.

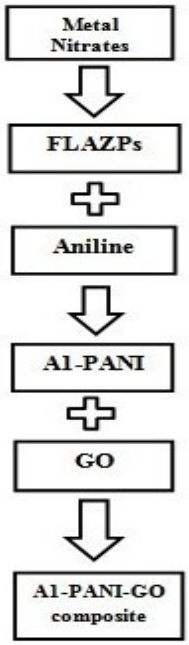

(A flow sheet summarizing the procedure of the whole synthesis process)

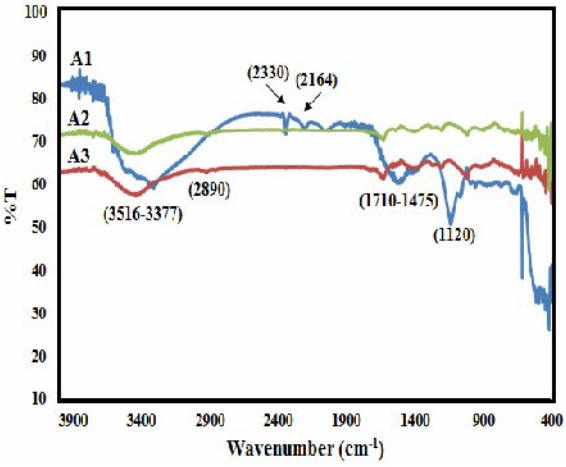

Fig. 1: FT-IR spectra of the prepared ceramic particles and composites.

Table-2: FT-IR Vibrational Assignments of the prepared Ceramic and its Composites.

Peak Position wavenumber (cm^{-1})			Concerned Vibrational Assignment
A1	A2	A3	
3377VS	3506W	3516W	O-H stretching
----	2890 VW	2890VW	C-N stretching
2330 S	---	---	O-H stretching
2164	---	---	Asym. N-H stretching
---	1710 S	1710 S	C=O stretching
1583 S	---	---	CO_2 stretching
---	1480 W	1475 W	C-N stretching
---	1284 W	1274 W	C-N stretching in quinoid ring
1120 VS	---	---	O-H deformation
1037 VW	1070 S	1060 W	C-H bending
950 W	930 W	941 W	$-CH_2$ wagging
840 W	---	---	N-O deformation
765 W	738 VW	730 VW	C=C in-plane vibration
615 S	621 W	630 W	O-H out of plane bending
524 W	561 W	550 W	C-C skeletal vibration
516 W	---	---	Fe-O stretching
430 W	403 W	420 W	Zn-O stretching

VS: Very strong, S: Strong, VW: Very weak, W: Weak

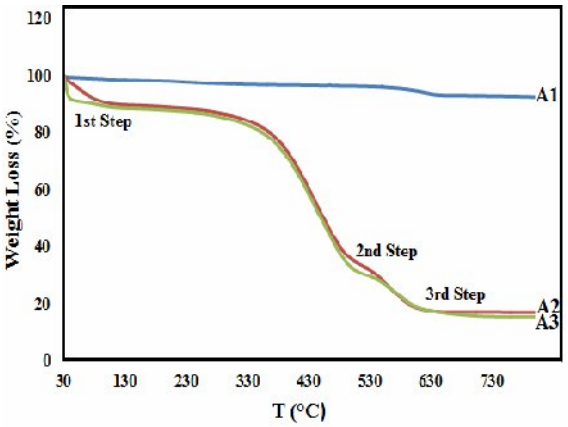

Fig. 2: Thermogramms of pure FLAZPs, FLAZPs-PANI and $FLAZP_S$-PANI-GO composites.

Thermal Analysis

To test the thermal stability of the composites, TGA analysis was conducted in the range from 30-800°C under nitrogen atmosphere as shown in Fig. 2. The results are summarized in Table-3. The TGA curve of A1 shows no apparent weight loss up to 600°C. However, a small drop at 115°C with 2.5% weight loss is primarily due to the evaporation of water molecules. The second drop at 600°C with 4% mass loss may be due to the formation of various phases of metal oxides in the material. The absence of clear degradation steps in the TGA curve of FLAZPs suggests the presence of strong ionic interactions between the metal ions (Fe, La, Al, Zn) in the ceramic composition. TGA curves of A2 and A3 show three main mass loss regions. The first drop at about 70-85°C (10%) is due to the loss of water and volatile gases from the samples. The second weight loss (60%) occurs at about 300-520°C demonstrates the decomposition of PANI and GO contents of the composites. Finally, the transition above 600°C represents the destabilization of the ceramic particles in both composites respectively. Improvement in the thermal stability of PANI and GO in the composites might be due to the formation of a defensive barrier against thermal decomposition [25]. The dispersion of A1 particles in the PANI/GO matrices enhances the stability of the composites as identified in SEM micrographs.

Table-3: Stepwise TGA data for the prepared materials.

Sample ID	1st step		2nd step		3rd step	
	T (°C)	W (%)	T (°C)	W (%)	T (°C)	W (%)
A1	115	2.5	---	---	600	4
A1/PANI	85	10	500	60	650	16
A1/PANI/GO	73	10	520	63	678	16

Morphology study

The surface morphology of the prepared samples A1, A2 and A3 was investigated by using SEM measurements as shown in Fig. 3. SEM micrographs of ceramic particles (A1) indicate spherical and rod shape crystallites with slight agglomeration. Particle size obtained from the image, ranges from 0.5µm to 500nm. The appearance of some porosity in these micrographs might be due to sintering process. These small and large pores are important for cell's in-growth in the crystallites [26]. The smooth morphology of A2 (A1-PANI) indicates the dispersion of ceramic particles in the polymer matrix. Furthermore, ceramic particles are firmly immobilized on the surface of GO in A3. The surface smoothness has been somewhat degraded in A3 which could possibly be due to the interaction between PANI and GO and the comparative dispersion of A1 particles in between the two matrices. There is a less agglomeration of A1 particles in A3 which may be due to the inhibition of agglomeration by GO. It should be noted that the absence of GO in A2 facilitated the dispersion of the particles in the polymer matrix. The degradation of smooth surface in A3 as compared to A2, shows the

overlapping of GO in the composit which might occur during the drying process of the sample. Holes and particulates on A3 surface as compared to A2, demonstrate the distribution of GO powder in PANI and ceramic composition [27]. Conversion of smooth (A2) into the porous (A3) morphology confirms the GO addition in the composite intercalated by interpenetrating networks of PANI wrapped A1 particles.

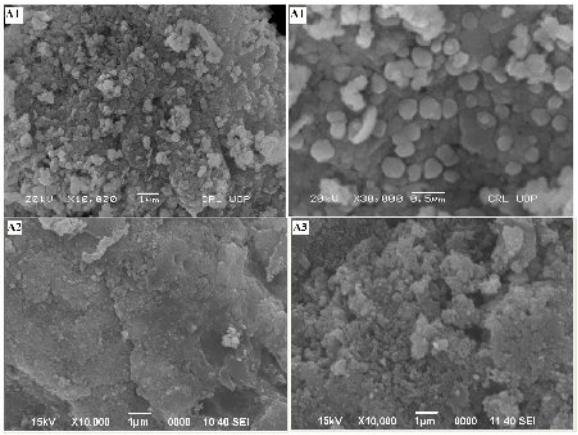

Fig. 3: SEM micrographs of FLAZPs (A1), LAZPs-PANI (A2) and FLAZPs-PANI-GO (A3).

XRD Analysis

Phase formation in the prepared samples was determined using XRD as shown in Fig. 4. The XRD pattern of A1 is comprised of well-resolved broad peaks which specify the absence of secondary phases. For ceramic particles (A1), the XRD peaks are well-indexed to the crystallographic planes at (100), (002), (101), (113), (102), (110), (103), (200) and (112). These planes signify the hexagonal wurtzite structure of ZnO with P63mc space group as identified from JCPDS card file No. 30-1451 [14]. Some undefined peaks in A1 pattern demonstrate the noise which might be caused by instrumental alignment. Diffraction pattern for ceramic-PANI composite (A2) shows characteristic peaks of PANI at 2θ = 14.200°, 17.050°, 26.750° and 28.300°. Due to the PANI-A1 interaction, peak intensities of the A1 at (100), (002), (101), (110) and (103) planes are suppressed with different ratios. This signifies the conversion of crystalline behavior of A1 particles into semi-crystalline shapes by the addition of the polymer. It is observed in the A2 diffraction pattern that the intensity of (200) peak is higher in case of composite which owes to the uniform distribution of A1 in PANI matrix [16]. A1 particles act as nucleation sites for PANI chains to pack together those results in the formation of large size crystallites. Also the increased peak intensity may be due to the increase in the volume content of A1 in PANI [16]. The accumulation of A1 particles on PANI substrate causes microstrain in the composite which results in the increase peak intensity. In A3, the addition of GO has suppressed the intensities of the retained ceramic peaks with different ratios and proportionalities that further decreased the crystallinity of the composite material. No peak is observed for GO in A3 pattern suggesting that GO has been reduced while interacting with ceramic particles as reported previously [22]. Also the absence of GO sharp peak may be attributed to the increase in interspace distance of graphene layer due to intercalation of A1-PANI between GO sheets. Peaks at 2θ = 26, 28 and 29° in A2 have been intensified in A3 which might be due to increasing inter-chain interaction between GO and PANI in the composite. However, composites as a whole acquire semi-crystalline structure.

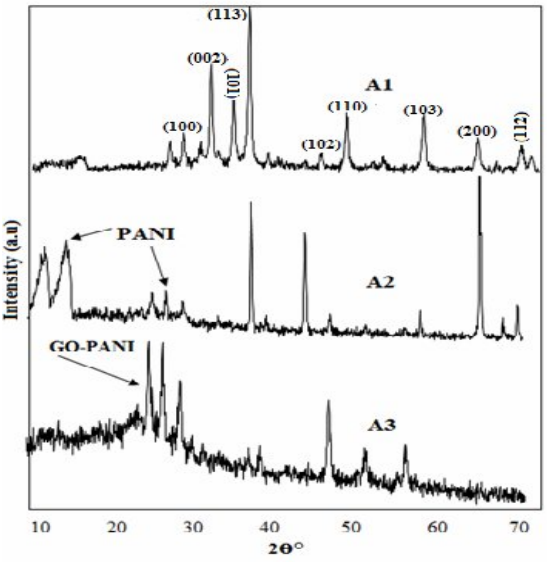

Fig. 4: XRD patterns for FLAZPs (A1) and its composites (A2 and A3).

Frequency Dependent Dielectric Properties

The development of dielectric properties (Figs. 5-7) was investigated in the frequency range from 1 MHz to 3 GHz at room temperature. The entire three important dielectric parameters *i.e.* dielectric constant (ε′), dielectric loss (ε″) and loss tangent (tan δ) exhibit a constant value in high frequency regions (up to 1.70 GHz) after which non-Debye (resonance) type behavior occurs. This may be due to the lack of coordination between the polarization of induced electric moments in the material and applied electric field frequency. High ε′ value of 2.27 at 1.6 MHz was observed for A3 sample. In Fig. 5, first resonance peak in both A2 and A3 arise at about 1.90 to 2.00 GHz respectively,

which may be attributed to the interfacial polarization. For A1, ε′ shows constancy due to higher levels of dielectric dispersion at low frequency [28]. The second, smaller peak in A1 at 2.49 GHz and a significant drop in A2 (at 2.54 GHz) and A3 (at 2.46 GHz) are ascribed to the trouble for dipoles to chase the switching fields with increasing frequency. Likewise, the dielectric loss due to polarization loss resulting in the rapid increase of loss tangent (tan δ) in the high frequency region as shown in Fig. 6 and 7 [13]. A high value 6.39 at 1 MHz for A3 shows that energy loss is more in this composite. However, both PANI and GO has the same additional effect on these properties [29].

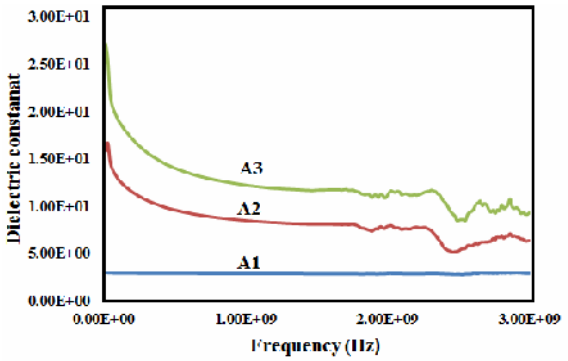

Fig. 5: Frequency dependence dielectric constant of the prepared FLAZPs and its composites at room temperature.

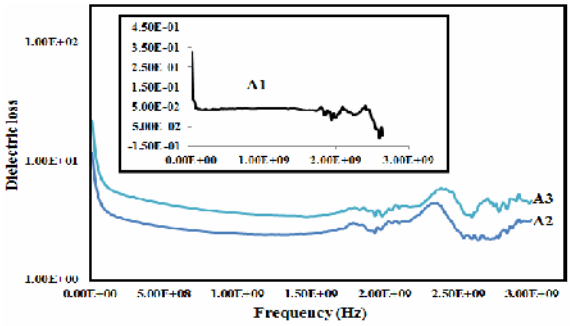

Fig. 6: Frequency dependence dielectric loss of the prepared FLAZPs and its composites at room temperature. (The inset represents the plot of pure FLAZPs).

AC conductivity of A1, A2 and A3 as a function of frequency at ambient temperature was determined using the following relation;

$$\sigma ac = \omega \varepsilon_{\circ} \varepsilon' \tan\delta \qquad (1)$$

where ω is the angular frequency (ω= 2πf), $\varepsilon_{\circ}$ is the permittivity of free space, ε′ is dielectric constant and tanδ is the loss tangent.

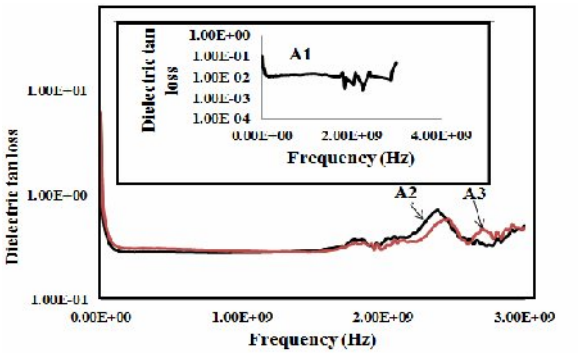

Fig. 7: Frequency dependence tan (permit) loss of the prepared composites at room temperature. (The inset represents the plot of pure FLAZPs).

Capacitance

Fig. 8 shows the variation of capacitance with frequency at ambient temperature. At low frequency (4.5 MHz), the capacitance has the highest value (1.43 PF). This is attributed to the decrease in the space charge region at the electrodes. Capacitance of A2 and A3 has decreased as frequency increased which may be due the partially blocked charge carriers near the electrodes.

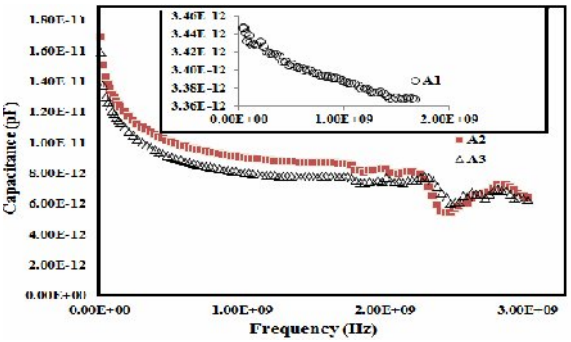

Fig. 8: Variation of capacitance with frequency of the prepared materials at room temperature.

Determination of AC Conductivity

Fig. 9 shows that *AC* conductivity for all the samples increases linearly with frequency up to 1.77-1.83 GHz. However, the conductivity of A2 and A3 is higher ($\sigma = 7.79 \times 10^{-1}\ \Omega^{-1}cm^{-1}$) than that of pure FLAZPs ($\sigma = 3.17 \times 10^{-1}\ \Omega^{-1}cm^{-1}$) which indicates the effect of conducting PANI and GO on the ceramic particles. At low frequency, ionic polarization displays *DC* component of conductivity. The frequency dependent *AC* conductivity behavior of these composites signifies the presence of dominant conductivity dispersion (hopping of electrons) in these materials. In this case a fraction of energy is

required for hopping as compared to activation of long range diffusive conductivity [29]. The resistance in all the prepared materials (Fig. 10) decreased with increasing current frequency. This demonstrates that with decreasing resistance, the possibility of charge carrier migration improves that in-turn enhances the conductance in the materials. The increase in resistance at about 2 and 3 GHz for A1 as is shown by the small peaks in the curve reflects its decrease in conductivity at these positions. Such peaks are not observed in A2 and A3 curves that clarify that PANI and GO enhanced the conductivity of ceramic particles.

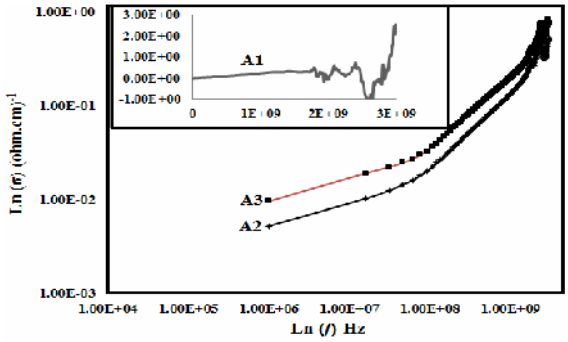

Fig. 9: Variation of AC conductivity with frequency of the prepared materials at room temperature.

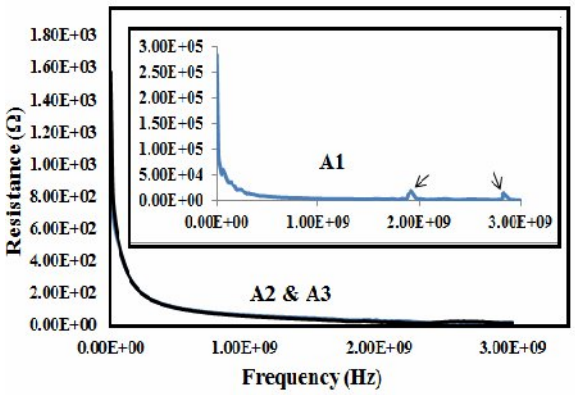

Fig. 10: Variation in resistance with frequency of the materials at room temperature.

Conclusions

Two-phase and three-phase polymer-graphene oxide-ceramic composites were successfully prepared using different synthesizing techniques. FT-IR results indicated the formation of two-phase and three-phase composites. SEM results declared the dispersion of ceramic particles and their size in the range from micro to nanometer. TGA analysis showed that ceramic particles have improved the thermal stability of PANI and GO in the composites. SEM micrographs indicated the distribution of the components in the composites. XRD analysis showed the phase distribution in the composites. The dielectric properties in the frequency range from 1 MHz to 3 GHz at room temperature showed that both the additives PANI and GO had added effects on the dielectric properties of FLAZPs. The *AC* conductivity (σ = 7.79 x 10^{-1} $\Omega^{-1}cm^{-1}$) achieved by the two-phase and three-phase composites is much higher in comparison to pure FLAZPs (σ = 3.17 x 10^{-1} $\Omega^{-1}cm^{-1}$).

Acknowledgments

The authors are grateful to the National Center of Excellence in Physical chemistry, University of Peshawar for financial assistance.

References

1. Y. Y. Yu, W. C. Chien, T. H. Wu and H. H. Yu, Highly Transparent Polimide/Nanocrystalline Titinia Hybrid Optical Materials for Antireflective Applications, *Thin Solid Films.,* **520**, 1495 (2011).
2. Y. Y. Yu, W. C. Chien, T. W. Tsai and H. H. Yu, Synthesis of Soluble Polyimide/Silica–Titania core–shell Nanoparticle Hybrid Thin Films for Anti-reflective Coatings, *Mater. Chem. Phys.,* **126**, 962 (2011).
3. Y. Y. Yu, W. C. Chien, J. M. Lin and H. H. Yu, High Transparent Polyimide/Titania Multilayer Anti-Reflective Hybrid Films, *Thin Solid Films.*, **519**, 4731 (2011).
4. B. T. Liu, S. J. Tang, Y. Y. Yu and S. H. Lin, Strength of the Interactions between Light-scattering Particles and Resins Affects the Haze of Anti-glare Films", Colloids and Surfaces A-Physicochemical and Engineering Aspects, *Colloid. Surface*. A., **377**, 138 (2011).
5. C. H. Park, H. S. Lee, K. H. Lee, D. H. Kim, H. R. Kim, G. H. Lee, J. H. Kimand S. Im, Organic/oxide Hybrid Complementary Thin-film Transistor Inverter in Vertical Stack for Logic, Photo-gating, and Ferroelectric Memory Operation*., Org. Electron.,* **12**, 1533 (2011).
6. S. Bichler, S. Feldbacher, R. Woods, V. Satzinger, V. Schmidt, G. Jakopic, G. Langer and W. Kern, Functional Flexible Organic–inorganic Hybrid Polymer for two Photon Patterning of Optical Waveguides, *Opt. Mater.,* **34**, 772 (2012).
7. F. Zhao, Z. Zhang, Y. Liu, Y. Dai, J. Chen and D. Ma, A Hybrid White Organic Light-Emitting Diode with Stable Color and Reduced Efficiency

Roll-off by Using a Bipolar Charge Carrier Switch, *Org. Electron.*, **13**, 1049 (2012).
8. N. Nakayama and T. Hayashi, Synthesis of Novel UV-Curable Difunctional Thirteen Methacrylate Plastic Lenses, *Prog. Org. Coat.,* **62**, 274 (2008).
9. C. H. Wua, H. Li, H. H. Fong, V. A. Pozdin, L. A. Estroff and G. G. Malliaras, Room-Temperature Preparation of Crystalline TiO_2 Thin Films and their Applications in Polymer/TiO_2 Hybrid Optoelectronic Devices*., Org. Electron.*, **12**, 1073 (2011).
10. M. S. Khan, R. Gul and M. S. Wahid, Studies on Thin Films of PVC-PMMA Blend Polymer Electrolytes*, J. Polym. Eng.,* **33**, 633 (2013).
11. J. W. Krumpfer, T. Schuster, M. Klapper and K. Müllen, Make it Nano-Keep it Nano*, Nano Today.*, **8**, 417 (2013).
12. T. Hanemann and D. V. Szabó, Polymer-Nanoparticle Composites: From Synthesis to Modern Applications, *Materials,* **3**, 3468 (2010).
13. J. Zhan, G. Tian, Z. Wu, S. Qi, and D. Wu, Preparation of Polyimide/BaTiO3/Ag Nanocomposite Films *via in situ* Technique and Study of Their Dielectric Behavior*., Chin. J. Polym. Sci.,* **32**, 424 (2014).
14. K. Shashi, K Susheel and K. Amit, A, A Novel Nanocomposite of Polyaniline and $Fe_{0.01}Ni_{0.01}Zn_{0.98}O$: Photocatalytic, Electrical and Antibacterial Properties*, J. Alloy. Compd.,* **578**, 249 (2013).
15. S. C. Tjong, Structural and Mechanical Properties of Polymer Nanocomposites*., Mat. Sci. Eng. R.,* **53**, 73 (2006).
16. K.. M. Sandeep, S. Bashiaah, K. C. J. Raju and V. V. S. S. Srikanth, Flexible Few-Layered Graphene/Poly vinyl Alcohol Composite Sheets: Synthesis, Characterization and EMI Shielding in X-Band through the Absorbtion Mechanism, *RSC Adv.,* **5**, 36498 (2015).
17. S. Patrizia, M. Mario, G. Mauro and T. Alberto, Analysis of Microwave Absorbing Properties of Epoxy MWCNT Composites*, Prog. Electromag. Res. Lett.,* **44**, 63 (2014).
18. X. Geng, D-W. He, Y. S. Wang, W. Zhao, Y. K. Zhou and S. L. Li, Synthesis and Microwave Absorption Properties of Graphene-Oxide (GO)/Polyaniline Nanocomposite with Fe_3O_4 Particles*, Chin. Phys.* B.*,* **24**, 27803 (2015).
19. P. Shaikshavali, K. R. Naresh, V. V. S. S. Srikanth, S. R. K. Bhanu, M. V. Reddy, P. L. Kian and B. V. R. Chowdari, Electrochemical Studies of Few –Layered Graphene as an Anode Material for Li ion Batteries, *J. Solid. Stat. Electrochem.,* **18**, 941 (2014).
20. Z. Zheng, Z. Xianhua, W. Haitao, and D. Qiangguo, Macroporous Graphene Oxide-Polymer Composite Prepared through Pickering High Internal Phase Emulsions, *ACS Appl. Mater. Interfaces.,***5**, 7974 (2013).
21. S. Jian, X. Liu, Z. Chunyang, X. Ruiqing, D. Qilin, L. Dali and S. Hongwei, Synthesis of Graphene Oxide Based CuO Nanoparticles Composite Electrode for Highly Enhanced Nonenzymatic Glucose Detection, *ACS Appl. Mater. Interfaces.,* **5**, 12928 (2013).
22. Z. Lu-Lu, D. Song, Y. Xue-Lin, P. Gang, L. Gan, H. Yun-Hui, J. Yan, N. Shi Bing and L. Ming, Reduced Graphene Oxide Modified Li_2FeiO_4/C Composite with Enhanced Electrchemical Performance as Cathode Material for Lithium Ion Batteries, *ACS Appl. Mater. Interfaces.,* **5**, 12304 (2013).
23. P. Shaikshavali, K. M. Sandeep, V. V. S. S. Srikanth, V. R. Mogalahalli and B. V. R. Chowdari, Elucidation of Few Layered Graphene-complex Metal Oxide ($A_2Mo_3O_8$, A = Co, Mn and Zn) Composites as Robust Anode Materials in Li ion Batteries, *Electrochem. Acta.,* **178**, 699 (2015).
24. R. V. Barde and S. A. Waghuley, Preparation and Electrical Conductivity of Novel Vanadate Borate Glass System Containing Graphene oxid*, J. Non-cryst. Solids.,* **376**, 117 (2013).
25. M. S. Khan and K. Gul, Preparation and Characterization of High Strength PMMA-Na_2SO_4 Composite Films, *Polym-Plast. Techno. Eng.,* **49**, 1347 (2010).
26. K. R. Mohamed, S. M. Mousa and G. T. El Bassyouni, Fabrication of Nano Structural Biphasic Materials from Phosphogypsum Waste and their In Vitro Applications, *Mat. Res. Bull.,* **50**, 432 (2014).
27. L. Guihua, S. Lei, Z. Gaofeng, Z. Yanfeng and S. Yuhan, Efficient Dehydration of the Organic Solvents through Graphene oxide GO/ceramic Composite Membranes, *RSC Adv.*, **4**, 52012 (2014).
28. M. N. Ashiq, R. B. Qureshi, M. A. Malana and M. F. Ihsan, Synthesis, Structural, Magnetic and Dielectric Properties of Zirconium Copper Doped M-type Calcium Strontium Hexaferrites, *J. Alloy. Compd.,* **617**, 437 (2014).
29. R. M. Al-Haddad, I. M. Ali, I. M. Ibrahim and M. A. Essa, DC and AC Conductivity Measurement of $Se_{60}Te_{30}Ge_{10}$ Films, *J. Al-Nahyan Uni. (Science).,* **12**, 72 (2009).